

0017-9310(95)00051-8

Convective heat transfer in periodic wavy passages

G. WANG and S. P. VANKA†

Department of Mechanical and Industrial Engineering, University of Illinois at Urbana-Champaign,
IL 61801, U.S.A.

(Received 1 July 1994 and in final form 19 January 1995)

Abstract—The rates of heat transfer for flow through a periodic array of wavy passages are studied with an accurate numerical scheme. The flow was observed to be steady until Re around 180 after which self-sustained oscillatory flow was observed. The self-sustained oscillations lead to the destabilization of laminar thermal boundary layers, replenish the near-wall fluid with the fluid in the core region, and thus provide a natural mechanism of heat and mass transfer enhancement. In the steady-flow regime, the average Nusselt numbers for the wavy wall channel were only slightly larger than those for a parallel-plate channel. On the other hand, in the transitional-flow regime, the enhancement of heat transfer was about a factor of 2.5. Friction factors for the wavy channel were about twice those for the parallel-plate channel in the steady-flow region, and remained almost constant in the transitional regime.

1. INTRODUCTION

There is a considerable amount of literature on methods to increase the rates of heat and mass transfer in compact exchange devices operated in the laminar flow regime [1]. The objective sought by these methods is to interrupt efficiently the boundary layer that forms on the exchange surface and replace it with fluid from the core, thereby creating a fresh boundary layer that has increased near-wall temperature (and concentration) gradients. Some examples of such techniques are off-set fins, louvers, vortex generators, communicating channels, acoustic excitation of the flow, oscillatory inflow, etc. The goal is to employ the technique that has the least pressure drop but the largest heat/mass transfer rate. However, other criteria such as simplicity, ease of manufacturability, dust collection in the passage, maintenance, scaling, etc., also become important. Applications of compact exchange devices abound in engineering, notably in the air-conditioning and refrigeration industry.

One geometry of the flow passage that is very simple and may be used to enhance the exchanger performance is that formed by wavy walls. Wavy channels are easy to fabricate and can provide significant heat transfer enhancement if operated in an appropriate (transitional) Reynolds-number range. Therefore, wavy passages have been considered in several earlier studies as a means to enhance heat/mass transfer in compact exchange devices. Both corrugated and converging-diverging cross-sections have been studied experimentally and numerically. An important observation made is that wavy passages do not provide any significant heat transfer enhancement when the flow

is steady. However, if the flow is made unsteady (either through external forcing or through natural transitioning to an unsteady state) significant increases in heat exchange are observed. This is a result of complex interactions between the core fluid and the boundary-layer fluid through shear-layer destabilization and self-sustained oscillations. It is in this regime that such passages can be very effective and our objective, therefore, has been to quantify such gains as well as penalties (increased pressure drop) through accurate and well-resolved numerical computations of the unsteady flow and heat exchange processes. A review of previous studies of wavy passages is given in Section 2. The steady regime does not provide any benefit, thus eliminating this passage as a possible augmentation device. However, we demonstrate (and confirm some earlier experimental studies) that a significant increase in heat transfer can be achieved when the flow changes to an unsteady self-sustained oscillatory state. Such self-sustained oscillations belong to a generic class of oscillations over cavities, studied extensively in aerodynamics. The transitional Reynolds number for the onset of these oscillations varies with flow geometry, but is typically low to be of interest to compact exchange devices.

Section 2 first provides an overview of contributions made by previous researchers on the present topic. Section 3 presents the governing equations and the numerical procedure. In the present study, a geometry that was earlier experimentally investigated by Nishimura *et al.* [2] has been considered. Both steady and unsteady regimes over a wide range of Reynolds numbers have been analysed. Section 4 describes the computational details and the grid sensitivity studies carried out to ensure numerical accuracy. Section 5 presents the steady characteristics, followed by Sec-

† Author to whom correspondence should be addressed.

NOMENCLATURE

a	amplitude of the wavy wall [m]	η	curvilinear coordinate
C_f	friction coefficient $\tau_w/(0.5\rho u_{av}^2)$	ζ	normalized vorticity $\omega H_{max}/u_{max}$
D_h	hydraulic diameter [m]	θ	dimensionless temperature ($T - T_w$)/($T_{m1} - T_w$)
f	friction factor $\Delta p H_{av}/(2\rho u_{av}^2 \lambda)$	Λ	source function in the energy equation [s ⁻¹]
h	heat transfer coefficient [W m ⁻² K ⁻¹]	λ	wavelength of the wavy wall [m]
H	inter-wall spacing [m]	ν	kinematic molecular viscosity [m ² s ⁻¹]
J	Jacobian of the coordinate transformation [m ²]	ξ	curvilinear coordinate
k	thermal conductivity [W m ⁻¹ K ⁻¹]	ρ	density [kg m ⁻³]
Nu	Nusselt number hD_h/k	τ	normalized time tu_{min}/H_{min}
p	pressure [N m ⁻²]	Φ	scalar potential [m ² s ⁻²]
Re	Reynolds number $u_{av}H_{av}/\nu$	ω	vorticity [s ⁻¹].
St	Strouhal number fD_h/u_{av}		
t	time [s]		
T	temperature [K]		
u	Cartesian velocity component in the x direction [m s ⁻¹]	Subscripts	
U	contravariant velocity component perpendicular to the lines of constant ξ [m ³ s ⁻¹]	av	quantity evaluated at the $\frac{1}{2}(H_{max} + H_{min})$ cross-section
v	Cartesian velocity component in the y direction [m s ⁻¹]	in	quantity evaluated at the inlet
V	contravariant velocity component perpendicular to the lines of constant η [m ³ s ⁻¹].	m	mean property evaluated at constant ξ lines
		m1	mean property evaluated at the inlet
		m2	mean property evaluated at the outlet
		max	quantity evaluated at the maximum cross-section
		min	quantity evaluated at the minimum cross-section
		n	number of the wave
		w	quantity evaluated at the wall.
Greek symbols			
α	thermal diffusivity [m ² s ⁻¹]		

tion 6 in which the unsteady features are described. Detailed pictorial descriptions of the unsteady flow and temperature fields that are responsible for the increased heat exchange are given along with quantitative data on friction factors and heat transfer rates. These results are, however, limited to one set of geometrical parameters and other sets in the parameter space may have somewhat different effectiveness. The exploration of the effects of such parameters can be an exhaustive research program and will be of an ongoing interest to us.

2. PREVIOUS RESEARCH

Viscous flow in wavy channels was first treated analytically by Burns and Parks [3]. The solution was obtained by expressing the stream function in a Fourier series under the assumption of Stokes flow. Vajravelu [4] studied the flow and heat transfer effects accounting for the convection contributions by a perturbation method using the long-wave approximation, where the solution consisted of a mean part and a perturbed part.

Goldstein and Sparrow [5] were probably the first to study the local and average heat/mass transfer characteristics for laminar, transitional, and low Reynolds number turbulent flow in a corrugated wall

channel. It was shown experimentally that, in the laminar regime upto a Reynolds number of 1000–1200, the transfer coefficients were only moderately larger than those for a parallel-plate channel. However, for the low Reynolds number turbulent flow ($Re = 6000$ – 8000), the rates of heat transfer exceeded those for the straight channel by nearly a factor of three. The corrugated channel had only two corrugation cycles, and thus those results were influenced by the entrance effects. O'Brien and Sparrow [6] studied the heat transfer characteristics in the fully developed region of a periodic channel in the Reynolds number range of $Re = 1500$ to $Re = 25000$. A level of heat transfer enhancement by about a factor of 2.5 over a conventional straight channel was observed, resulting from a highly complex flow pattern including a strong forward flow and an oppositely directed recirculating flow. The effects of varying the spacing between the corrugated walls was examined by Sparrow and Comb [7] in the Reynolds number range of 2000 to 27000. The increase of the inter-wall spacing gave rise to a 30% increase in the fully developed Nusselt number compared with that of O'Brien and Sparrow [6], but the friction factor was more than doubled.

Ali and Ramadhyani [8] recently conducted an experimental study in corrugated channels of planar cross-section in the steady and transitional Reynolds

number regimes ($150 < Re < 4000$). Flow visualization studies indicated the appearance of longitudinal vortices, as the Reynolds number was progressively increased. Furthermore, it was observed that in the transitional regime, spanwise vortical structures rolled up from the shear layers at a regular frequency corresponding to a Strouhal number ($St = fD_h/u_{av}$) between 0.8 and 1.1. These spanwise eddies transfer near-wall fluid to the core region and enhance the rate of heat transfer. Performance evaluations under the constraints of equal pressure drop, equal mass flow and equal pumping power all indicated that corrugated channels operated at transitional Reynolds numbers provide superior rates of heat transfer. It was also observed that the channel wall spacing has an appreciable effect on the onset of transition to an unsteady flow. Numerical studies of steady flow and heat transfer in corrugated channels have been conducted by Garg and Maji [9], Amano *et al.* [10], Asako and Faghri [11] and Asako *et al.* [12].

Sparrow and Prata [13] conducted experimental and numerical studies of flow and heat transfer in a symmetric triangular wavy wall. The experimental study was limited to Reynolds numbers below 200 and did not show any heat transfer enhancement over the straight tube value. The numerical study solved the steady-state flow and energy equations and also did not reveal any increase in heat transfer even at Reynolds numbers of 1000. However, in the turbulent regime ($Re = 6000\text{--}70\,000$), it was seen [14] that the rates of heat transfer are much larger than those in an equivalent straight tube. Even after discounting the additional pressure drop resulting from larger wall shear, wavy passages were found to provide enhanced heat transfer.

Flow characteristics in a channel with a symmetric sinusoidal wavy wall were investigated experimentally and numerically by Nishimura *et al.* [2]. In the laminar flow regime, the friction factor was observed to be inversely proportional to Reynolds number, but in the transitional and turbulent regimes it was independent of Reynolds number. Furthermore, there is small peak in the friction factor curve which was accredited to the flow transition. The numerical prediction of the pressure drop was in good agreement with the measured values until about $Re = 350$. Nishimura *et al.* [15, 16] also studied the mass transfer coefficients at high Peclet numbers for the same channel, and the mass transfer mechanism was interpreted on the basis of the flow results. For steady flow, no enhancement in mass transfer was observed, but the increase was remarkable once the flow became unsteady. The friction factor remained constant instead of decreasing with Reynolds number. In a comparative assessment of three lateral alignments of the waves, Nishimura *et al.* [17] inferred that the corrugated channel offered slightly better performance over furrowed channels. However, only one set of amplitude and wavelength

was considered and the observations made could be different if these were varied.

There were several other studies related to this problem. Sobey [18] presented the flow pattern for steady and oscillatory flow in a channel with sinusoidal wavy walls in order to understand the performance of the Oxford membrane oxygenator (Bellhouse *et al.* [19]) and to determine the details of the flow structure. Stephanoff *et al.* [20] qualitatively confirmed the numerical results of Sobey by demonstrating visually the process of vortical formation, growth and subsequent ejection from a furrow. Sobey [21, 22] further predicted the quasi-steady solution in the small Strouhal number region and the expansion of vortices during a deceleration in asymmetric channels, with the Strouhal number sufficiently large for the flow not to be quasi-steady. Ralph [23] investigated the oscillatory viscous flow in a wavy-walled tube for Strouhal numbers between 0.025 and 0.045 and reported the development of time-asymmetric flow. The occurrence of time asymmetry was regarded as a bifurcation of the flow structure in this Strouhal number range. Stephanoff [24] conducted an experimental study on self-excited shear-layer oscillations in a multi-cavity channel similar to the earlier numerical [18] and experimental [20] investigations. The experiment was held at constant mean velocity, and the selective amplification of a single frequency was observed. Recently Guzmán and Amon [25] conducted simulations of the transition process from laminar to chaotic flow using a spectral element method. The transition path to chaos was characterized and the corresponding streamline development was illustrated. These results are similar to some of the observations of our current study.

Although not directly related to the present work, there have been several numerical studies of transport phenomena in grooved and communicating channels [26–30]. The conclusions of these studies are similar to those in wavy passages, namely that significant heat transfer enhancement can be obtained at super-critical Reynolds numbers while also minimizing the dissipation due to viscous stresses. There also exist several Japanese experimental and numerical studies in sinusoidal wavy channels [31–34], which we have not been able to access because of the language of publication.

The present study provides a systematic quantitative characterization of the forced convective heat transfer processes in a wavy passage.

3. CONSERVATION EQUATIONS AND NUMERICAL PROCEDURE

In the present study, the flow is considered to be two-dimensional with no variation in the spanwise direction. The governing equations for the flow and energy transport can be written as :

$$\nabla \cdot \mathbf{u} = 0 \quad (1)$$

$$\frac{\partial \mathbf{u}}{\partial t} + \nabla \cdot (\mathbf{u}\mathbf{u}) = -\nabla p + \nu \nabla^2 \mathbf{u} \quad (2)$$

$$\frac{\partial \theta}{\partial t} + \theta \Lambda + \nabla \cdot (\mathbf{u}\theta) = \alpha \nabla^2 \theta \quad (3)$$

where $\theta = (T - T_w)/(T_{m1} - T_w)$, and ν and α are the kinematic viscosity and the thermal diffusivity respectively. Here, T_w is the wall temperature and T_{m1} is the mixed mean fluid temperature (mass averaged temperature) evaluated at the inlet section of the computational domain. The unknown function Λ in the energy equation is given by

$$\Lambda = \frac{1}{T_{m1} - T_w} \frac{\partial}{\partial t} (T_{m1} - T_w). \quad (4)$$

This term results from the present normalization procedure as T_{m1} is a function of time when the flow is unsteady, and it can be determined iteratively. We have also assumed the density to be unity.

These conservation equations are solved on a curvilinear orthogonal grid. The orthogonal mesh is generated by a general case of sequential mapping [35], i.e. by solving

$$x_{\xi\xi} + x_{\eta\eta} = 0 \quad \text{and} \quad y_{\xi\xi} + y_{\eta\eta} = 0 \quad (5)$$

to generate the interior mesh points. A boundary value for x or y is computed from the orthogonality constraint, and the other coordinate value is then determined by the relation describing the shape of the boundary [36].

The numerical integration of the above equations is based on a two-stage fractional step procedure with backward Euler differencing of the time derivative and Adams–Bashforth explicit differencing for the convection terms. The Crank–Nicolson implicit scheme is used for the diffusion terms. In a fractional step procedure, the first stage of the integration consists of solving the momentum equations for an intermediate velocity field $\hat{\mathbf{u}}$ given by

$$\frac{\hat{\mathbf{u}} - \mathbf{u}^n}{\Delta t} = \frac{3}{2} \mathbf{H}^n - \frac{1}{2} \mathbf{H}^{n-1} + \frac{\nu}{2} \nabla^2 [\hat{\mathbf{u}} + \mathbf{u}^n] \quad (6)$$

where $\mathbf{H} = -\nabla \cdot (\mathbf{u}\mathbf{u})$ and Δt is the time step size. This step is followed by the solution of a Poisson equation for Φ

$$\nabla \cdot [\nabla \Phi] = \frac{1}{\Delta t} \nabla \cdot \hat{\mathbf{u}} \quad (7)$$

such that

$$\mathbf{u}^{n+1} = \hat{\mathbf{u}} - \nabla \Phi \Delta t \quad (8)$$

satisfies the divergence free condition imposed by the mass continuity equation. The pressure field is related to the scalar potential Φ by the relation

$$p^{n+1} = \Phi^{n+1} - \frac{\nu \Delta t}{2} \nabla^2 \Phi^{n+1}. \quad (9)$$

The implicit momentum equations for the two velocity components (\hat{u}, \hat{v}) are solved with a two-step

operator splitting procedure involving line inversions along the two (ξ and η) directions. For the line inversion along the ξ direction, periodic boundary conditions are used while Dirichlet conditions are used at the no-slip walls in the η direction. The pressure Poisson equation is solved with the multigrid technique [37] using a point Jacobi iterative procedure and a V-cycle correction scheme. Because of the uniform cell sizes and nearly isotropic coefficients, rapid convergence, typically in less than 15 V-cycles is obtained with several levels of grid coarsening.

The determination of the temperature distribution is made complicated by the presence of the unknown function Λ in the energy equation. The coupling between θ and Λ can be solved iteratively. First, the energy equation is solved with proper boundary conditions and a guessed value of Λ . Then, the inlet temperature, θ_{in} is adjusted to satisfy the constraint that the mean temperature θ_{m1} is unity at the entrance. A new value of Λ is computed by summing finite-difference equations in the η direction at the inlet. This calculation procedure is repeated until a converged solution is obtained.

The spatial discretization uses a collocated arrangement with the two Cartesian velocities and the pressure situated at the centers of discrete finite volumes in the computational domain. The continuity equation is satisfied by the mass fluxes located at the cell faces. These volume fluxes (U and V) are related to the Cartesian velocities (u and v) by

$$U = J(\xi_x u + \xi_y v) \quad (10)$$

$$V = J(\eta_x u + \eta_y v) \quad (11)$$

where ξ_x , ξ_y , η_x and η_y are the metrics of the transformation and J is the Jacobian. The values of \hat{U} and \hat{V} are evaluated from \hat{u} and \hat{v} at the cell centers. After corrections by the gradient of Φ , U and V satisfy mass continuity to the convergence accuracy of the pressure solution. However, the cell-centered u and v , even after the corrections, do not satisfy the mass continuity equation precisely, but the error is of the same order as the error in the spatial discretization. The boundary conditions and the details of the computation are provided in the next section.

4. COMPUTATIONAL DETAILS

All calculations presented in this paper were performed for a geometry with dimensions shown in Fig. 1 which corresponds to the geometry in the experimental study of Nishimura *et al.* [2]. Two plates with sinusoidal waves are placed with a mean spacing of 1.3 units. Each wave has an amplitude-to-length ratio ($2a/\lambda$) of 0.25 and a wavelength of 2.8 units. As boundary conditions, no slip conditions are prescribed for the Cartesian velocities together with a constant wall temperature condition for the energy equation. Thus,

$$u_w = 0, \quad v_w = 0, \quad \theta_w = 0. \quad (12)$$

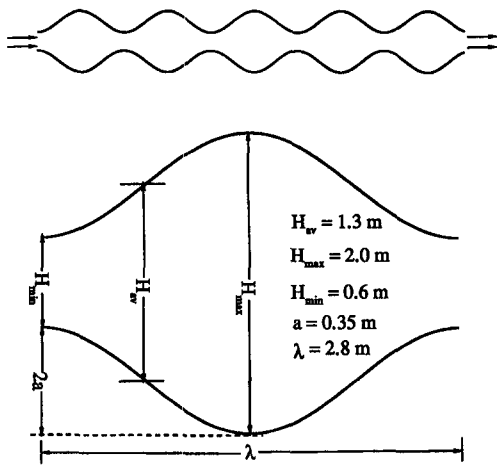


Fig. 1. Geometry of the sinusoidal wavy wall channel.

In the streamwise direction, periodic conditions of the form

$$\begin{aligned} u(0, y, t) &= u(n\lambda, y, t) \\ v(0, y, t) &= v(n\lambda, y, t) \\ \frac{\theta(0, y, t)}{\theta_{m1}} &= \frac{\theta(n\lambda, y, t)}{\theta_{m2}(t)} \end{aligned} \quad (13)$$

are used. Here, n denotes the number of the wave and λ is the wavelength. θ_{m1} and θ_{m2} are the non-dimensional mass averaged temperatures at the inlet and the outlet of the computational domain. The imposition of periodicity for the temperature profile is similar to the specification of a fully developed condition in a circular pipe, as presented in Kays and Crawford [38]. For the pressure equation, no boundary conditions are necessary at the walls as the cell face fluxes are known (to be zero) directly on the walls. However, wall pressures are still necessary in updating the cell-centered Cartesian velocities and, in the present algorithm, these are obtained by a zero normal derivative condition. In the streamwise direction, a constant pressure drop is specified, i.e.

$$p(n\lambda, y) - p(0, y) = 20n\lambda v. \quad (14)$$

An alternative condition will be to specify the mass flow through the channel. Here we have considered the pressure-drop condition. The Prandtl number was taken to be 0.7.

Systematic grid refinement studies have been conducted to ensure numerical accuracy of the results. Calculations have been conducted with grids containing 64×32 , 128×64 , and 256×128 internal cells over one wavelength of the wave. Calculations are performed for various Reynolds numbers, ranging from the steady regime to the unsteady regime and comparisons of the flow and temperature profiles as well as the Nusselt number and friction factor have been made. In the steady regime, good accuracy was obtained with the 64×32 grid. However, in the unsteady regime, a slight difference was observed

between the results of the two finer grids. The finest grid with 256×128 cells was selected in all calculations presented in this paper. Finer grids were not considered because of the computational costs. The effect of the streamwise length at which periodicity conditions were imposed was also studied by considering a computational domain of three wavelengths. In this case, a mesh of 768×128 cells was used. No differences were observed between the instantaneous flow patterns in individual furrows, thus demonstrating the adequacy of using only one of the waves as the computational domain. This observation is consistent with that of Amon and Mikic [26] for a channel with a rectangular groove.

5. RESULTS FOR THE STEADY REGIME

A systematic progression in Reynolds number was obtained by decreasing the fluid kinematic viscosity ν . This also decreased the pressure drop through the channel appropriately to simulate a nearly linear decrease of friction factor with Reynolds number. (Because the kinematic viscosity was the independent variable, the Reynolds numbers actually obtained did not turn out to be integer values.) Although in the steady regime the flow is symmetrical about the horizontal centerline, requiring only the solution for one of the halves, the complete domain (between the two walls) was solved in order to locate the transition from the steady regime to the unsteady regime (where the flow is unsymmetric). The discretized equations were integrated for a sufficiently long time until a time invariant flow field was obtained. This convergence was monitored through successive changes in velocities at representative positions. All calculations presented in this paper were obtained with the finest grid. Figure 2 shows the calculated streamlines at Reynolds numbers of 5.4, 20.6, 80.5 and 144.0. At $Re = 5.4$, the streamlines are nearly symmetrical about the vertical center line and no separation is observed. This indicates that the nonlinear convection terms are relatively small compared with the diffusion effects. With increase in Reynolds number, the streamlines become asymmetrical about the vertical center line. The flow is first seen to separate at $Re = 20.6$, with steady vortices formed upstream of the crest of the upper wall (and the trough of the lower wall). With further increase in the Reynolds number, the recirculation zones increase in size and shift downstream. The maximum stream function, normalized by the mean velocity (u_{av}) and half of the averaged channel height (H_{av}) increases, reflecting the growth of separation bubbles that are associated with negative flow.

Figure 3(a) presents comparisons of the calculated separation and reattachment points with the experimental data of Nishimura *et al.* [2] as a function of the Reynolds number. The calculated results are based on the steady-state solution in the steady regime and part of the transitional regime. The locations of the

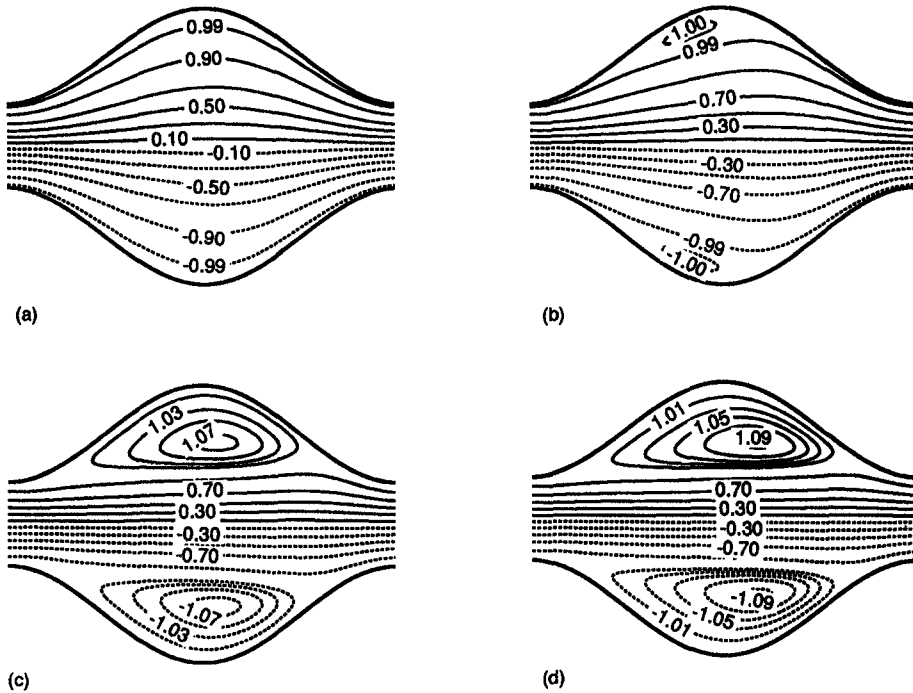


Fig. 2. Contours of stream functions at various Reynolds numbers: (a) $Re = 5.4$; (b) $Re = 20.6$; (c) $Re = 80.5$; (d) $Re = 144.0$.

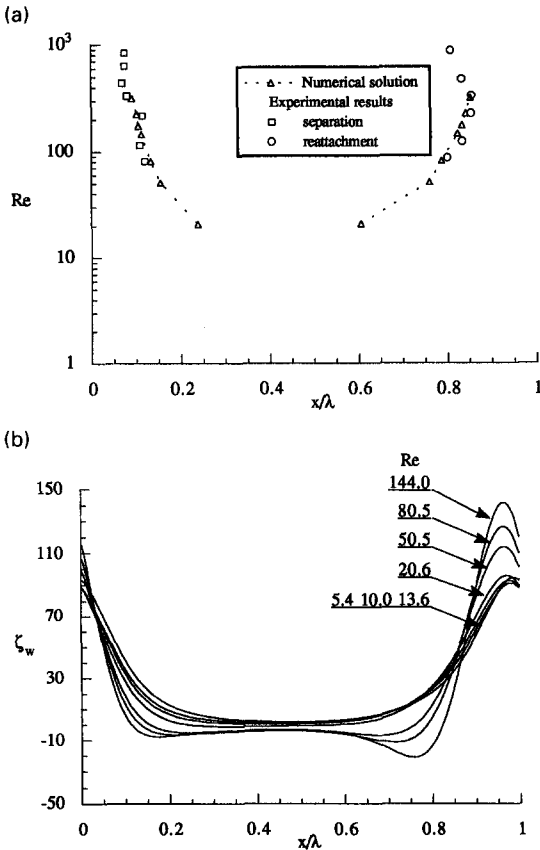


Fig. 3. (a) Variation in separation and reattachment points with Reynolds number. (b) Calculated wall vorticity profiles at various Reynolds numbers.

separation and reattachment points are determined from the sign of the near-wall vorticity. The present results agree well with experiments, demonstrating the accuracy of the numerical solutions and the grid employed. The wall friction coefficient, C_f is assigned a positive value for forward flow and a negative value for reverse flow. The observed distributions are consistent with the streamline patterns presented earlier. As the Reynolds number is increased, the peak friction coefficient decreases but the minimum remains almost constant.

The distributions of the normalized wall vorticity, ζ_w are shown in Fig. 3(b). To be consistent with the work of Nishimura *et al.* [2], the vorticity ω is normalized by the maximum channel height H_{max} and the corresponding local bulk velocity u_{max} , i.e.

$$\zeta_w = \frac{\omega_w}{u_{max}/H_{max}} = \frac{1}{2} Re C_f \left(\frac{H_{max}}{H_{av}} \right)^2. \quad (15)$$

At very low Reynolds numbers, the wall vorticity is positive everywhere. As the flow separates from the walls, negative vorticity corresponding to the negative velocity is seen. The magnitudes of both the maximum and minimum wall vorticities increase with the Reynolds number.

Figure 4 presents the temperature contours for the same Reynolds numbers. At $Re = 5.4$, the temperature drops quickly because of diffusion from the walls. A thermal boundary layer develops along the walls. As the Reynolds number increases, the temperature pro-

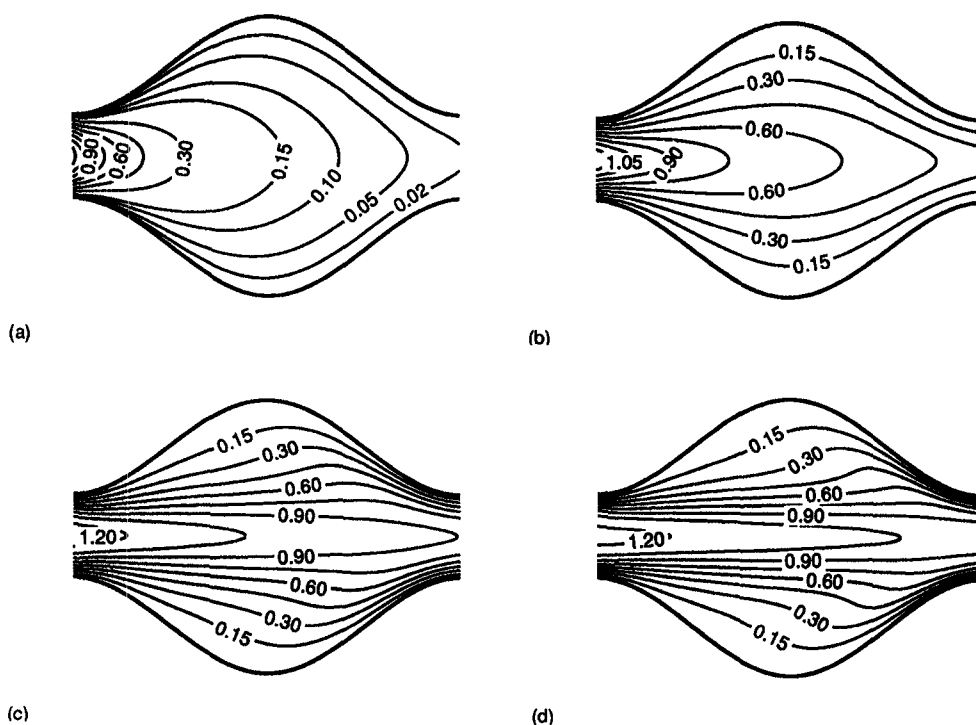


Fig. 4. Contours of normalized temperature at various Reynolds numbers: (a) $Re = 5.4$; (b) $Re = 20.6$; (c) $Re = 80.5$; (d) $Re = 144.0$.

files start to be distorted in the recirculation region. Consequently, the thermal boundary layer has been destroyed by the eddies. It is seen that the temperature gradient near the reattachment point is much greater than that near the separation point.

Figure 5(a) presents the Nusselt number distributions for the various Reynolds numbers. The local Nusselt number is defined as

$$Nu = \frac{hD_h}{k} = \frac{D_h}{\theta_m(\xi)} \frac{\partial \theta}{\partial n} \quad (16)$$

where h is the convection heat transfer coefficient, D_h is the hydraulic diameter of the wavy channel (which is equal to twice the average channel height, H_{av}) and $\theta_m(\xi)$ is the bulk mean temperature evaluated at constant ξ lines. The maximum and minimum Nusselt numbers are located near the minimum and maximum cross-sections of the passage, respectively. The difference between the maximum and minimum Nusselt numbers is seen to increase with the Reynolds number as the temperature gradients become steeper near the minimum cross-section. However, as shown in Fig. 5(b), the overall heat transfer coefficient does not increase much because the Nusselt number in the minimum cross section has a relatively small contribution.

6. RESULTS IN THE UNSTEADY FLOW REGIME

Near the transition, the constant mass flow with pressure periodic boundary condition was used as it

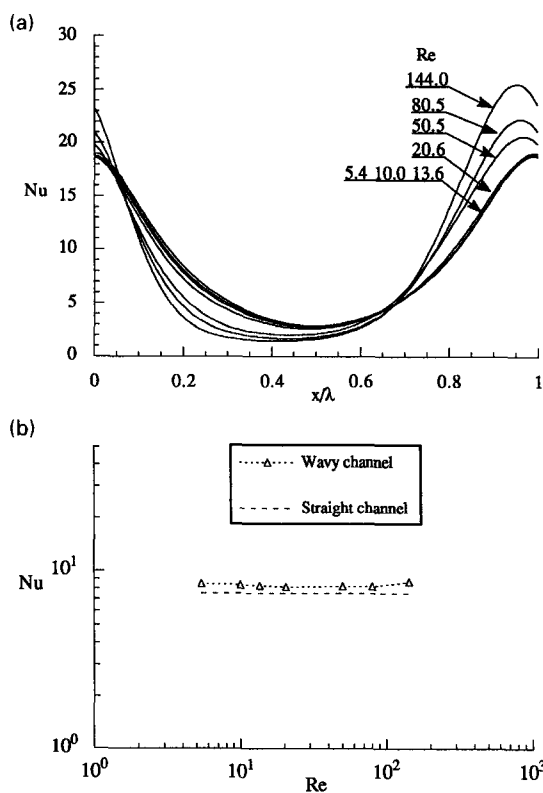


Fig. 5. (a) Variation of local Nusselt number at various Reynolds numbers in the steady regime. (b) Variation of Nusselt number with Reynolds number in the steady regime.

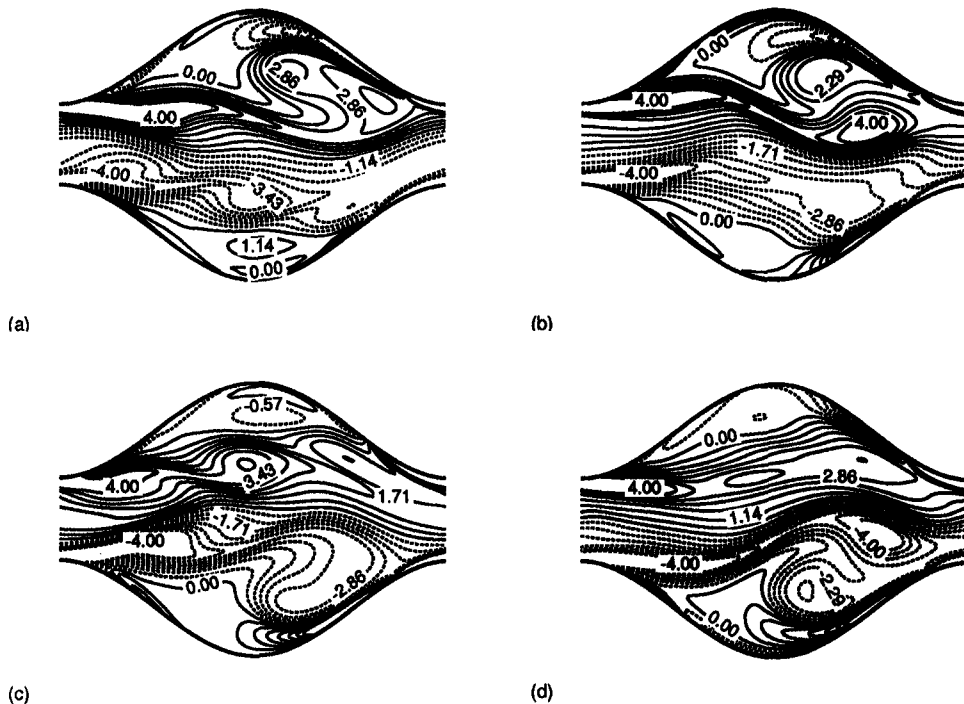


Fig. 6. A typical cycle of the vorticity dynamics at Reynolds number of 328: (a) $\tau = 178.0$; (b) $\tau = 181.5$; (c) $\tau = 185.0$; (d) $\tau = 188.5$.

has the advantage of a direct control of Reynolds number. At $Re = 167$, the results converge to their steady state. The least-stable mode is oscillatory with a frequency which matches the frequency of the least-stable Tollmien–Schlichting mode for a plane channel flow. At a higher Reynolds number of $Re = 200$, the flow becomes unsteady and bifurcates to a periodic attractor. The phase portrait of v vs u at a point approaches a limit cycle. As the Reynolds number is further increased, a new characteristic frequency appears and the flow exhibits a quasiperiodic behavior. This transition scenario has recently been discussed in detail by Guzmán and Amon [25]. However, our recent study indicates that the transition scenario also depends on the periodic boundary conditions employed in the numerical procedure.

The oscillatory and enhanced heat transfer is the result of the destabilization of the separation bubbles by the vortices rolled up from the shear layers. This instability of the shear layers is similar to that observed in grooved channels and can be classified to be of Kelvin–Helmholtz type. Figure 6 shows a typical cycle of the vorticity dynamics at a nominal Reynolds number of 328. The unsteady nature of the upper and lower shear layers can be clearly seen in these figures. At $\tau = 178$, the roll-up of the upper shear layer is more clearly evident. This vortex is convected into the next periodic passage by $\tau = 185$ and a new vortex begins to form. The dynamics of the bottom shear layer are similar but differ in phase by approximately seven time units from those of the upper shear layer. It has been observed that the vorticity plot at $\tau = 192$

is nearly identical to that at $\tau = 178$. It can be seen that in a given half of the domain, both clockwise and counter clockwise vortices exist and evolve in a complex manner. At $\tau = 178$, there is a region of negative vorticity close to the upper wall (dotted lines), separated by the shear layer with positive (counter clockwise) vorticity. The negative vorticity is a remnant in time of a separation bubble formed in the wavy cavity at an earlier instant that is slowly engulfed by the shear layer. This interaction of the core fluid with the fluid in the cavities replenishes the thermal boundary layer and results in enhanced heat transfer. The corresponding temperature fields at these time instances are shown in Fig. 7. At $\tau = 178$, we see that large temperature gradients exist at the upper wall. This is a result of the core fluid penetrating into the cavity region as the shear layer rolls up into a vortex. At $\tau = 181.5$, the vortex moves deeper into the cavity and further entrains the previously formed thermal boundary layer. As the upper shear layer convects into the next wavy passage, the bottom shear layer now entrains the boundary layer in the lower cavity. These temperature plots may be compared with those in the steady region at $Re = 144$ which illustrate the differences between the steady and unsteady processes. The variation of the Nusselt number at the upper and lower surfaces along with their average is shown in Fig. 8. The Nusselt number is averaged over one wavelength of either the higher or the lower surface. It can be seen that the Nusselt number fluctuates quasiperiodically with an average considerably higher than the steady value. Although the individual

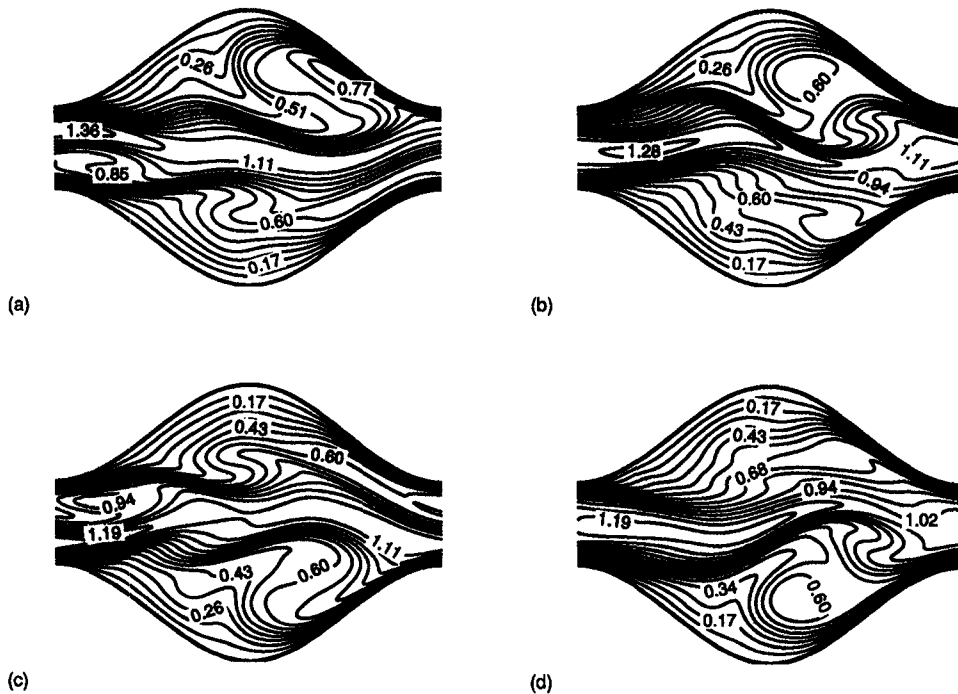


Fig. 7. The temperature fields at Reynolds number of 328: (a) $\tau = 178.0$; (b) $\tau = 181.5$; (c) $\tau = 185.0$; (d) $\tau = 188.5$.

variations are large, because of their being out of phase, the variations in the average are not large. At $Re = 328$, the time-averaged Nusselt number is approximately twice that at $Re = 144$.

As the Reynolds number is further increased, the dynamics of the flow become more complex, resulting in tearing of the vortices from the shear layers. Figure 9 shows the contours of vorticity at $Re = 520$ at four instances. Corresponding temperatures plots are presented in Fig. 10. It can be seen that the major increase in heat transfer occurs in the downstream half of the passage where the tip of the shear layer rolls up and curls towards the walls. The dynamics of the vortices at $Re = 520$ are significantly more complex than at

$Re = 328$ as the shear layer breaks into individual vortices.

Figure 11(a) shows the overall Nusselt number $\langle Nu \rangle$ for the unsteady regime. There is a significant increase in Nu over the straight channel value of 7.54 at these Reynolds numbers. Thus, wavy passages can be effective heat transfer enhancement devices at these transitional Reynolds numbers.

The heat transfer enhancement is accompanied by an increase in the pressure drop compared with the planar channel values. Figure 11(b) shows the friction factor as a function of Reynolds number. In the steady regime, the friction factor is approximately twice that of the planar channel. The increase in the pressure drop results from larger wall shear in the converging sections. The present calculations slightly under-predict the experimental data of Nishimura *et al.* [2], but show very good agreement with the experimental trends.

7. CONCLUSIONS

Flow patterns and heat transfer characteristics in a sinusoidally curved converging-diverging channel have been investigated through accurate numerical solutions of the governing equations on a curvilinear orthogonal grid. The wavy channel studied corresponds to the geometry of Nishimura *et al.* [2]. For Reynolds numbers less than 180, steady laminar flow is observed. Beyond this value a transition to chaotic flow accompanied by significant increase in heat trans-

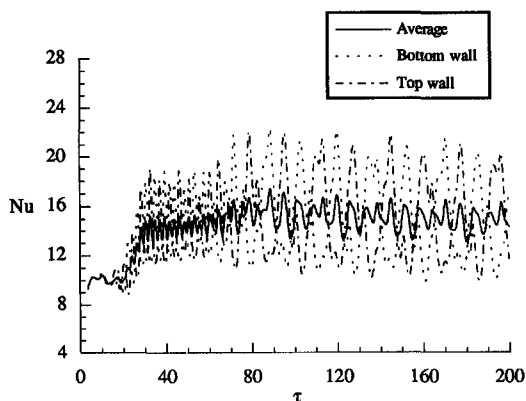


Fig. 8. Variation of Nusselt number with time for $Re = 328$.

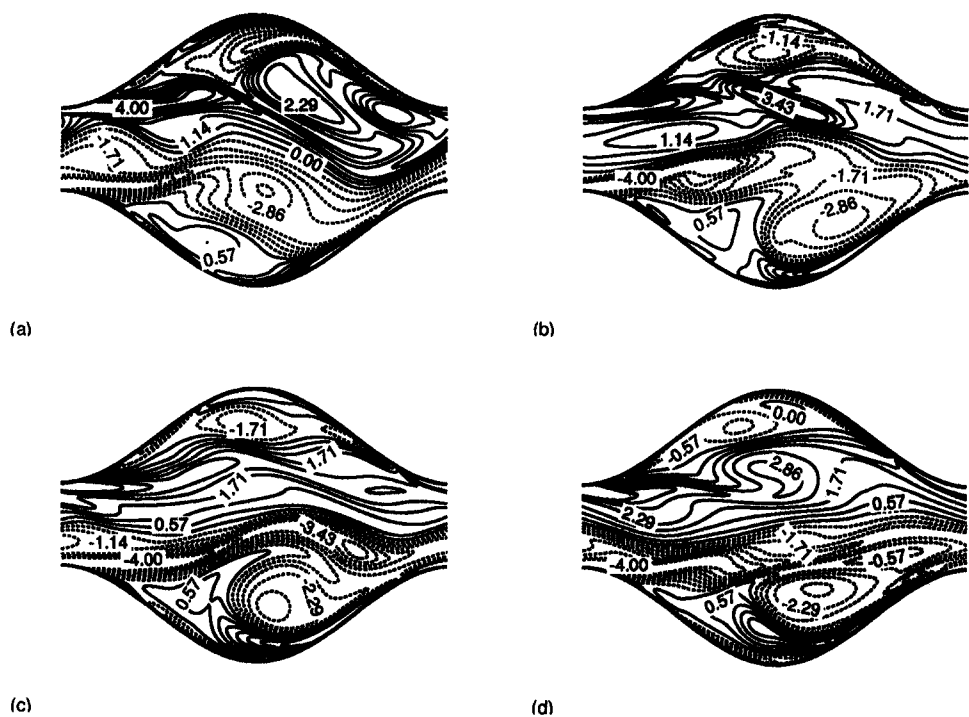


Fig. 9. Contours of vorticity at $Re = 520$ at four time instances: (a) $\tau = 140.0$; (b) $\tau = 143.0$; (c) $\tau = 146.0$; (d) $\tau = 149.0$.

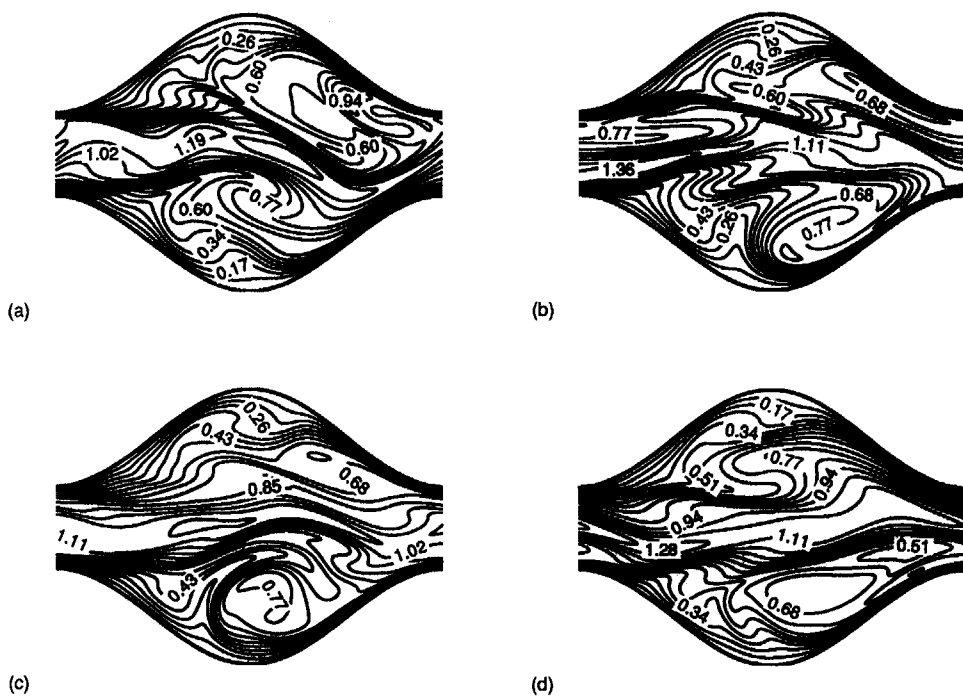


Fig. 10. Contours of temperature at $Re = 520$ at four time instances: (a) $\tau = 140.0$; (b) $\tau = 143.0$; (c) $\tau = 146.0$; (d) $\tau = 149.0$.

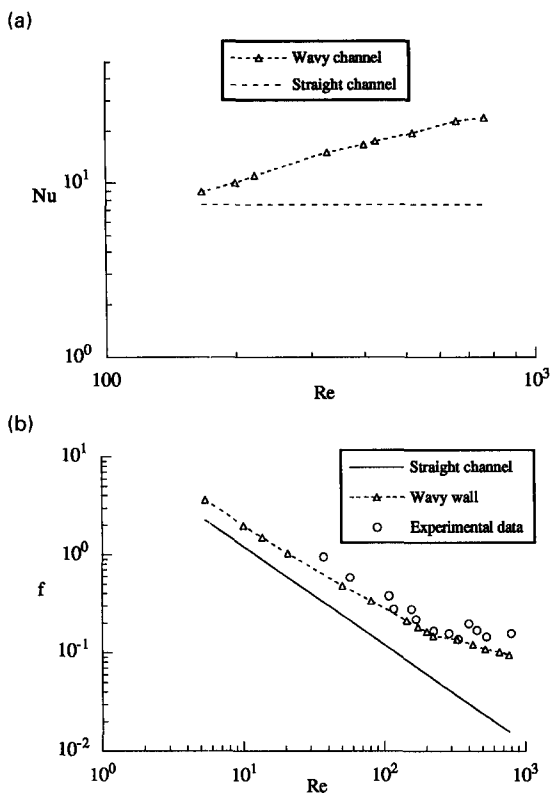


Fig. 11. (a) Variation of Nusselt number with Reynolds number in the unsteady regime. (b) Variation of friction factor with Reynolds number in the steady and unsteady regimes.

fer is observed. This enhancement in the heat transfer results from self-sustaining oscillations which lead to the destabilization of the laminar thermal boundary layers.

REFERENCES

1. R. L. Webb, *Principles of Enhanced Heat Transfer*, Wiley, New York (1994).
2. T. Nishimura, Y. Ohori and Y. Kawamura, Flow characteristics in a channel with symmetric wavy wall for steady flow, *J. Chem. Engng Jap.* **17**, 466–471 (1984).
3. J. C. Burns and T. Parks, Peristaltic motion, *J. Fluid Mech.* **29**, 405–416 (1967).
4. K. Vajravelu, Fluid flow and heat transfer in horizontal wavy channels, *Acta Mech.* **35**, 245–258 (1980).
5. J. L. Goldstein and E. M. Sparrow, Heat/mass transfer characteristics for flow in a corrugated wall channel, *J. Heat Transfer* **99**, 187–195 (1977).
6. J. E. O'Brien and E. M. Sparrow, Corrugated-duct heat transfer, pressure drop, and flow visualization, *J. Heat Transfer* **104**, 410–416 (1982).
7. E. M. Sparrow and J. W. Comb, Effect of interwall spacing and fluid flow inlet conditions on corrugated-wall heat exchanger, *Int. J. Heat Mass Transfer* **26**, 993–1005 (1983).
8. M. M. Ali and S. Ramadhyani, Experiments on Convective Heat Transfer in Corrugated Channels, *Expl Heat Transfer*, **5**, 175–193 (1992).
9. V. K. Garg and P. K. Maji, Flow and heat transfer in a sinusoidally curved channel, *Int. J. Engng Fluid Mechanics* **1**, 293–319 (1988).
10. R. S. Amano, A. Bagherlee, R. J. Smith and T. G. Neiss, Turbulent heat transfer in corrugated channels with and without fins, *J. Heat Transfer*, **109**, 62–67 (1987).
11. Y. Asako and M. Faghri, Finite-volume solutions for laminar flow and heat transfer in a corrugated duct, *J. Heat Transfer* **109**, 627–634 (1987).
12. Y. Asako, H. Nakamura and M. Faghri, Heat transfer and pressure drop characteristics in a corrugated duct with rounded corners, *Int. J. Heat Mass Transfer* **31**, 1237–1245 (1988).
13. E. M. Sparrow and A. T. Prata, Numerical solutions for laminar flow and heat transfer in a periodically converging-diverging tube, with experimental confirmation, *Numer. Heat Transfer* **6**, 441–461 (1983).
14. P. S. Mendes and E. M. Sparrow, Periodically converging-diverging tubes and their turbulent heat transfer, pressure drop, fluid flow, and enhancement characteristics, *J. Heat Transfer* **106**, 55–63 (1984).
15. T. Nishimura, Y. Ohori and Y. Kawamura, Mass transfer characteristics in a channel with symmetric wavy wall for steady flow, *J. Chem. Engng Jap.* **18**, 550–555 (1985).
16. T. Nishimura, S. Murakami, S. Arakawa and Y. Kawamura, Flow observations and mass transfer characteristics in symmetrical wavy-walled channels at moderate Reynolds numbers for steady flow, *Int. J. Heat Mass Transfer* **33**, 835–845 (1990).
17. T. Nishimura, Y. Kajimoto and Y. Kawamura, Mass transfer enhancement in channels with a wavy wall, *J. Chem. Engng Jap.* **19**, 142–144 (1986).
18. I. J. Sobey, On flow through furrowed channels. Part 1. Calculated flow patterns, *J. Fluid Mech.* **96**, 1–26 (1980).
19. B. J. Bellhouse, F. H. Bellhouse, C. M. Curl, T. I. MacMillan, A. J. Gunning, E. H. Spratt, S. B. MacMurray and J. M. Nelems, A high efficiency membrane oxygenator and pulsatile pumping system, and its application to animal trial, *Trans. Am. Soc. Artif. Intern. Organs* **19**, 72–79 (1973).
20. K. D. Stephanoff, I. J. Sobey and B. J. Bellhouse, On flow through furrowed channels. Part 2. Observed flow patterns, *J. Fluid Mech.* **96**, 27–32 (1980).
21. I. J. Sobey, Oscillatory flows at intermediate Strouhal number in asymmetric channels, *J. Fluid Mech.* **125**, 359–373 (1982).
22. I. J. Sobey, The occurrence of separation in oscillatory flow, *J. Fluid Mech.* **134**, 247–257 (1983).
23. M. E. Ralph, Oscillatory flows in wavy-walled tubes, *J. Fluid Mech.* **168**, 515–540 (1986).
24. K. D. Stephanoff, Self-excited shear-layer oscillations in a multi-cavity channel with a steady mean velocity, *J. Fluids Engng* **108**, 338–342 (1986).
25. A. M. Guzmán and C. H. Amon, Transition to chaos in converging-diverging channel flows: Ruelle-Takens-Newhouse scenario, *Phys. Fluid* **6**, 1994–2002 (1994).
26. C. H. Amon and B. B. Mikic, Numerical prediction of convective heat transfer in self-sustained oscillatory flows, *J. Thermophys.* **4**, 239–246 (1990).
27. C. H. Amon and B. B. Mikic, Spectral element simulations of unsteady forced convective heat transfer: application to compact heat exchanger geometries, *Numer. Heat Transfer* **19**, 1–19 (1991).
28. N. Ghaddar, M. Magen, B. B. Mikic and A. T. Patera, Numerical investigation of incompressible flow in grooved channels. Part 2. Resonance and oscillatory heat transfer enhancement, *J. Fluid Mech.* **168**, 541–567 (1986).
29. N. K. Ghaddar, K. Z. Korczak, B. B. Mikic and A. T. Patera, Numerical investigation of incompressible flow in grooved channels. Part 1. Stability and self-sustained oscillations, *J. Fluid Mech.* **163**, 99–127 (1986).
30. G. E. Karniadakis, B. B. Mikic and A. T. Patera, Minimum-dissipation transport enhancement by flow destabilization: Reynolds analogy revisited, *J. Fluid Mech.* **192**, 365–391 (1988).

31. T. Chiba, M. R. Ektesabi, N. Fukushima and M. Sako, Heat transfer characteristics for turbulent flow in wavy sinusoidal channels, *Preprint of 24th Symposium Heat Transfer Society of Japan* (in Japanese), p. 58 (1986).
32. R. S. Amano, A. Bagherlee, R. J. Smith and T. G. Niess, Turbulent heat transfer in a channel of wavy-fin plates, *Preprint of 23th Symposium Heat Transfer Society of Japan* (in Japanese), p. 352 (1986).
33. R. Izumi, H. Yamashita and K. Oyakawa, Flow and heat transfer in corrugated wall channels (3rd Report), *Trans. Jpn. Soc. Mech. Engng* (in Japanese), **48**, 1994 (1982).
34. K. Oyakawa, T. Shinzato and I. Mabuchi, The effects of the channel width on heat-transfer augmentation in a sinusoidal wave channel, *JSME Int. J.* **32**, 403–410 (1989).
35. C. Temperton, Direct methods for the solution of the discrete Poisson equation: some comparisons, *J. Comput. Phys.* **31**, 1–20 (1979).
36. J. F. Thompson, Z. U. A. Warsi and C. W. Mastin, *Numerical Grid Generation: Foundations and Applications*. Elsevier, Amsterdam (1985).
37. A. Brandt, Multi-level adaptive solutions to boundary-value problems, *Math. Comput.* **31**, 333–390 (1977).
38. W. M. Kays and M. E. Crawford, *Convective Heat and Mass Transfer*. McGraw-Hill, New York (1980).